第 33 卷第 9 期
2021 年 9 月

强 激 光 与 粒 子 束
HIGH POWER LASER AND PARTICLE BEAMS

Vol. 33，No. 9
Sep.，2021

·Particle Beams and Accelerator Technology·

Drive laser shaping and transport system for photocathode RF gun

Li Cheng， Wang Wenxing， Li Weiwei， Zhang Haoran， Jiang Shimin， Gao Panyun， He Zhigang， Zhang Shancai

（*National Synchrotron Radiation Laboratory*, *University of Science and Technology of China*, *Hefei* 230029, *China*）

Abstract: To meet the requirements of Hefei Advanced Light Facility (HALF) for high quality injection beam, a photocathode RF gun is developed as the electron source of the injector in the R&D project. To obtaining an electron beam with high qualities, it is necessary to carry out experimental research on drive laser shaping and transport system. For suppressing the beam emittance growth caused by space charge force, the temporal pulse shape is modified by using birefringent crystals, while an aperture is used for spatial pulse shaping. An optical image transport system is designed to achieve high stability of the laser beam position on the photocathode. Detailed design of the optical system is presented in this paper. The experimental result shows that a quasi uniform distribution in the three-dimensional space of laser pulse is obtained, and the laser beam position jitter on the photocathode is less than 4 μm. The performance of the laser pulse meets the experiment requirements.

Key words: photocathode RF gun； laser shaping； birefringent crystals； transport system； emittance

CLC number: TL503.3 **Document code:** A **doi**: 10.11884/HPLPB202133.210091

The photocathode RF gun uses an ultra-fast drive laser to illuminate the photocathode and produces an electron beam with the corresponding distribution through the photoelectric effect. Then the electron beam experiences the RF electric field in the cavity, its energy is rapidly increased to several MeV. The photocathode RF gun can provide a high brightness electron source (brightness: $B \propto q/\varepsilon_n^2\sigma_t\sigma_v$) with low emittance ($\varepsilon_n$), high peak current (high charge q, short bunch length σ_t), and low energy spread (σ_v); At the same time, since the electron beam produced by the photocathode has a sub-fs response time, the generated electron beam is strictly synchronized with the laser pulse. Due to the above advantages, the photocathode RF gun is widely used in short-wavelength free-electron lasers[1](FELs), ultra-fast electron detection (diffraction imaging[2], transmission imaging[3], pulse radiolysis[4]), Compton scattering sources[5](X-ray/γ-ray) and so on.

Among the performance parameters of the photocathode RF gun, transverse emittance is the most critical one. An electron bunch with 100 pC and ps width is dominated by spacecharge forces. How to reduce the emittance growth caused by the space charge effect is the key. Laser shaping technique is an effective way, which has been verified by theoretical analysis and experimental results[5-7].

Laser shaping includes temporal shaping and spatial shaping. The techniques used for temporal shaping depend strongly on the duration of the initial laser pulse. When the laser pulse has a duration longer than 1 ns, it can be shaped directly by electro-optic modulators[8-10]. For a femtosecond laser pulse, it can be shaped by modulating the amplitude and phase in the spectral domain using optical devices[11-13]. Due to the narrow spectrum, spectral modulation is difficult for picosecond pulses; Besides, due to the limitation of electronic system bandwidth, it is not feasible to shape the pulse directly by electro-optic modulators. Although acousto-optic modulators with a programmable dispersion filter[14-15](DAZZLER) have successfully shaped the picosecond pulses, their low optical-power handling capabilities make them applicable only to low repetition rate and the output may contain residual spatiotemporal distortions. In most cases, pulse stacking technique is used to temporally shape the picosecond pulses of hertz to megahertz repetition rate. Pulse stackers can be constructed with conventional delay lines[16] or birefringent crystals[17-19]. The conventional delay line consists of various and a large number of optical elements, such

* **Received date:** 2021-03-18； **Revised date:** 2021-08-24
Foundation item: Hefei Advanced Light Facility R&D Project
Biography: Li Cheng, lc199622@mail.ustc.edu.cn.
Corresponding author: He Zhigang, hezhg@mail.ustc.edu.cn.

as polarization beam splitters, polarizers, half-wave plates, mirrors, etc., which require high alignment accuracy. Pulse stacking with birefringent crystals is simple and compact. Although the flexibility is limited, it can provide a stable output. Likewise, there are many methods for spatial pulse shaping, such as refractive shapers[20-21], microlens arrays[22-23], deformable mirrors[24], and so on. In particular, although the optical loss is relatively large, using an aperture to obtain a truncated-Gaussian spatial profile is simple and easy to implement. Moreover, the experimental results show that a truncated-Gaussian[25-26] profile can produce an electron beam with a smaller emittance than that of a uniform distribution[26].

The position stability of the laser pulse on the photocathode will also affect the beam emittance and the position and angle stability of the beam emitted from the electron gun. Designing a high-stability laser transport system is also essential to obtain high quality electron beams.

In this paper, we use three α-BBO crystals and an aperture to obtain a laser pulse with temporally uniform distribution and spatially truncated-Gaussian distribution. Since the photoinjector of an accelerator is located at a few meters away from the laser room, we designed and built an image transport system to deliver the shaped laser beam onto the photocathode at 6 m away from the aperture. And the measured spatial position jitter of the laser pulse is less than 4 μm.

1 Overall layout of the optical system

The laser system (Coherent Inc.) consists of 3 main parts: oscillator, amplifier, and third harmonic generator, and their specific parameters are shown in Table 1 respectively.

Table 1 Laser parameters

element	wavelength/nm	pulse width/fs	repetition rate/Hz	pulse energy/nJ
oscillator	800	42	79.33×10^{6}	9
amplifier	800	10^{3}	1−100	13×10^{6}
third harmonic generator	266.7	1.5×10^{3}	1−100	2×10^{6}

The overall layout of the optical system is shown in Fig. 1. The oscillator emits a horizontally polarized laser at central wavelength of 800 nm and a pulse width of 42 fs. It is divided into two beams through a 50/50 beam splitter, one of which is used for the cross-correlation scanning measurements, and the other is sent to the amplifier to produce an amplified laser with a

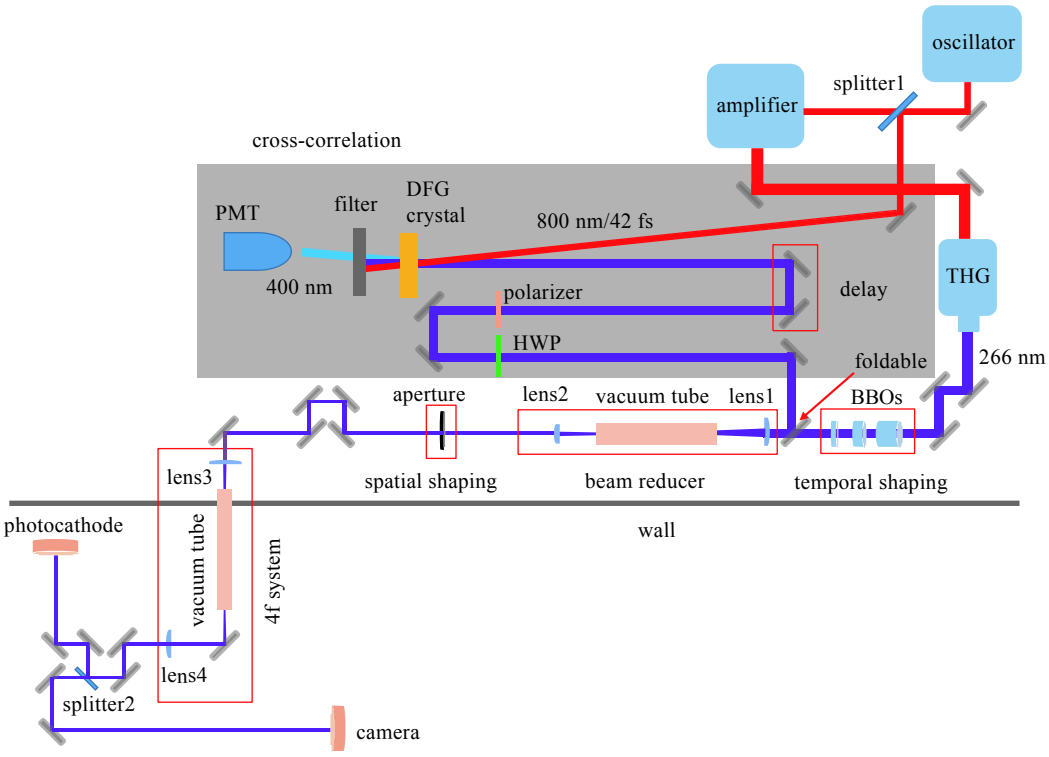

Fig. 1 Schematic diagram of the overall laser optical system

pulse width of about 1 ps. The repetition rate of the laser is adjustable in the range of 1−100 Hz. Then the amplified infrared laser pulse passes through a third harmonic generator to produce a 266.7 nm horizontally polarized ultraviolet (UV) laser. The UV laser pulse firstly pass through three α-BBO crystals to form a flat-top distribution in temporal domain.Then a beam reducer is used to reduce the beam size. Downstream the beam reducer, there is a spatial shaping aperture to obtain a truncated-Gaussian profile, which is transported to the photocathode through the 4f system. In the transport system, a 5% beam splitter (i.e. splitter2) is introduced for virtual cathode monitoring.

2 Optical design and experimental results of the pulse shaping and transport system

2.1 Temporal pulse shaping

α-BBO crystal is an excellent birefringent material with high transmittance and large birefringence over the wavelength range of 190−3500 nm. The Sellmeier equations of α-BBO crystal can be expressed as follows

$$\begin{cases} n_{\mathrm{o}}(\lambda) = \sqrt{2.747\,1 + \dfrac{0.018\,78}{\lambda^2 - 0.018\,22} - 0.013\,54\lambda^2} \\ n_{\mathrm{e}}(\lambda) = \sqrt{2.317\,4 + \dfrac{0.012\,24}{\lambda^2 - 0.016\,77} - 0.015\,16\lambda^2} \end{cases} \tag{1}$$

where the unit of λ is μm. The relationship between the group refractive index and the refractive index is

$$n_{\mathrm{g}} = n - \lambda \frac{\mathrm{d}n}{\mathrm{d}\lambda} \tag{2}$$

where n_{g} represents the group refractive index, and n represents the refractive index.

Assuming that the angle between the polarization direction of the pulse and the optical axis is Ψ, after passing through the α-BBO crystal, the electric field amplitude ratio of the o-ray (component perpendicular to the optical axis) and e-ray (component parallel to the optical axis) is $\tan\Psi$. To ensure that the intensity of the two pulses is equal, Ψ should be +45° or −45°.

Refractive indexes of the two pulses in the crystal are different, which cause their propagation speed to be different, and the temporal separation Δt introduced by the crystal of length L can be expressed as follows

$$\frac{\Delta t}{L} = \frac{1}{v_{\mathrm{og}}} - \frac{1}{v_{\mathrm{eg}}} = \frac{n_{\mathrm{og}} - n_{\mathrm{eg}}}{c} \tag{3}$$

where v_{og} and v_{eg} are the group velocities for the o-ray and e-ray respectively, c is the speed of light in vacuum, and n_{og} and n_{eg} are the group index of refraction for the o-ray and e-ray respectively.

For the UV laser at central wavelength 266.7 nm, n_{og} = 2.031 and n_{eg} = 1.778. Then it can be calculated as $\Delta t/L$ = 0.84 ps/mm. That is, a crystal with a thickness of 1 mm can introduce a 0.84 ps temporal separation.

Generally, using m birefringent crystals can transform a single Gaussian pulse into a stack of 2^m Gaussian output pulses. Fig. 2 shows a schematic diagram of temporal shaping using three α-BBO crystals, in which the red line represents the polarization direction of the laser pulse and the optical axis of the crystal. The horizontally polarized laser pulse passes through the first crystal (the optical axis oriented at 45° relative to the horizontal direction) and then it is divided into two sub-pulses with equal intensity. For α-BBO (a negative uniaxial crystal), the e-ray will move ahead of the o-ray. After passing through the second crystal (the optical axis oriented at 90° relative to the horizontal direction), each sub-pulse is divided into two sub-pulses, thus producing four sub-pulses with equal intensity. Finally, the four sub-pulses pass through the third crystal (the optical axis oriented at 45° relative to horizontal direction) to produce eight sub-pulses with alternate polarizations. To get micro-pulses with equal interval, the thickness of the latter crystal should be half or twice as the former one. Here we set the thickness of the first crystal to be L, then the thickness of the second and third crystal to be $L/2$ and $L/4$ respectively. According to the width of the initial laser pulse, we design the pulse interval to be 1.512 ps, corresponding to the thickness of the third crystal as 1.8 mm

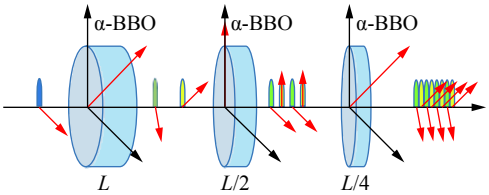

Fig. 2 Schematic diagram of pulse stacking scheme

and the total thickness of the three crystals as 12.6 mm. The transmittance of α-BBO crystal will decrease as the thickness of the crystal increases. According to the measurement, the total transmittance of the three crystals is about 45%. The influence of the dispersive material needs to be considered. In the optical system, three kinds of dispersive materials are included: α-BBO crystals used for pulse stacking, CaF_2 lenses used for beam reducer and 4f systems, and fused silica windows used at both ends of the vacuum pipe. The total material dispersion was calculated as 0.01039 ps^2 and 0.00667 ps^2 for the o-ray and e-rayrespectively, which is negligible for ps pulses.

To measure the temporal distribution precisely, the cross-correlation scanning method is used. In the experiment, using the shaped pulse and an IR pulse to irradiate the β-BBO crystal at a small angle, then a 400 nm signal is generated by difference frequency generation (DFG) in the crystal (type I, o + o = e, 0.2 mm , θ = 46.5°). A half-wave plate and polarizer placed after the stacker enable us to rotate the polarization of the output pulse to match the polarization of the IR pulse. A high-sensitivity photomultiplier tube (PMT) is used to detect the 400 nm signal. The cross-correlation profile is obtained by a multishot measurement scanning the delay of the pulse. We reduce the amplitude jitter by averaging on many shots per delay position. The resolution of the system is limited by the step length of the delay line and the IR pulse width. The minimum step of the translation stage we use can reach 0.05 μm, so the measurement accuracy depends on the IR pulse width is 42 fs.

Fig. 3 shows the theoretical and experimental results. The measured RMS intensity fluctuation of the shaped pulse is 7.7%, the rise time is about 1 ps, and the fall time is about 1.27 ps.

As can be seen in Fig. 3, there is a difference between the theoretical results and experimental results, which comes from several aspects. First, the temporal distribution of the initial pulse is not perfectly Gaussian. Second, the actual thickness of each crystal has a relatively large deviation from the theoretical design. It is best to control the tolerance within ± 0.01 mm. Third, the adjustment precision of the crystal holder is not good enough (only 2°). It is necessary to replace it with a higher-precision crystal rotation holder.

2.2 Spatial pulse shaping and transport system

As shown in Fig. 1, after temporal shaping, the input laser beam is reduced by using a 2.5× beam reducer, and the laser beam radius becomes 2.12 mm ($1/e^2$). Then an aperture with a diameter of 2 mm is used to obtain a truncated-Gaussian profile, which is transported to the photocathode through the 4f system.

We use plano-convex lenses of focal length +160 mm and +400 mm for the beam reducer and two plano-convex lenses of focal length +1500 mm for the 4f system. Simulation results of the laser beam transport system are shown in Fig. 4.

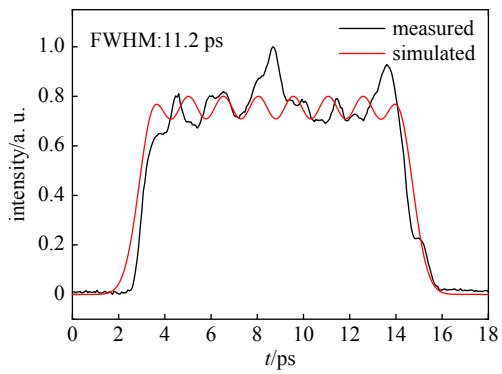

Fig. 3 Temporal profiles of laser pulse

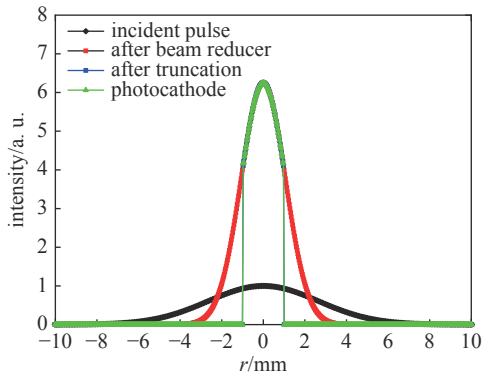

Fig. 4 Designed spatial profiles of laser pulse

It can be seen that the optical components we selected can well transport the truncated-Gaussian pulse to the photocathode.

As shown in Fig. 5, the spatial distribution of the laser pulse is measured at different positions. At the designed position, an image of the pulse transport through the aperture can be observed. At other positions, diffraction patterns appear as a fringe structure imposed on the actual spatial distribution. At the range of plus or minus 5 cm from the designed positions, we can observe that the diffraction is not obvious, which is beneficial to the construction of the optical system.

At the focal point of the lens, the laser power density is very high, which will cause air ionization. For this reason, we installed a vacuum tube in the focusing light path. Vacuum windows need to be added at both ends of the vacuum tubes. The

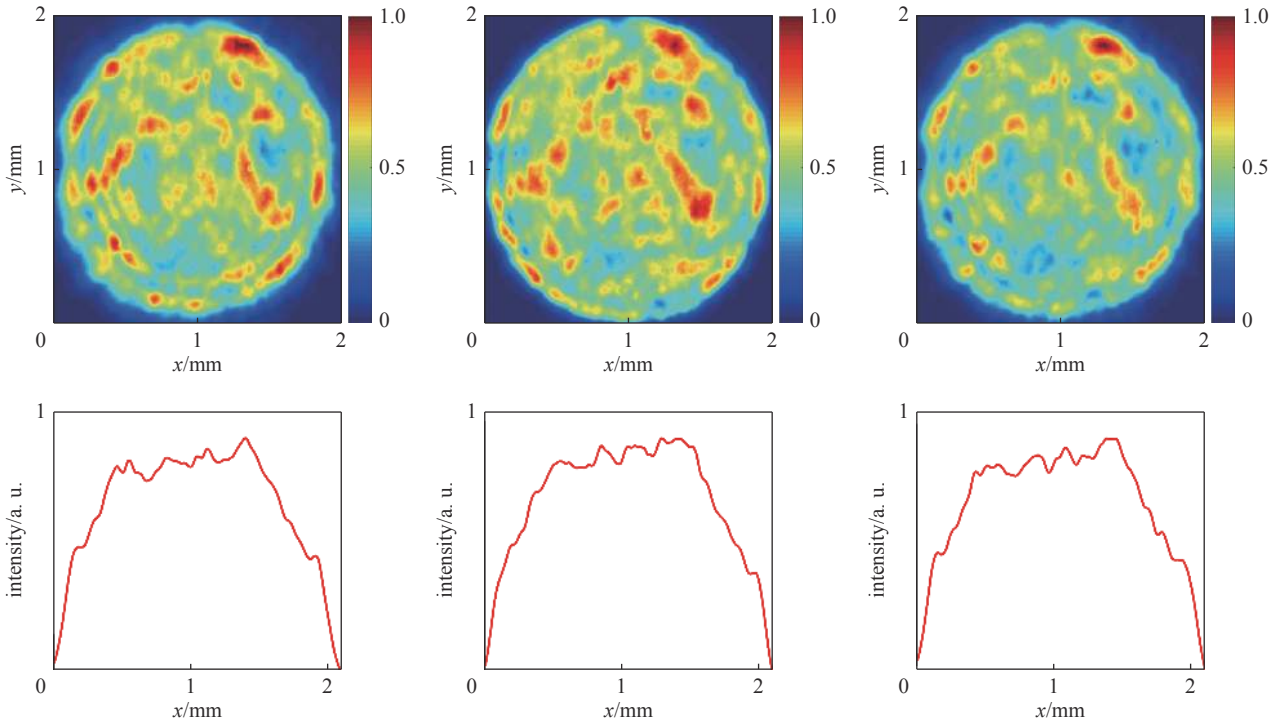

Fig. 5 Measured transverse distributions (upper) and horizontal cuts (lower) of laser pulse at different positions around the nominal imaging plane. From left to right, the distances to the nominal imaging plane are −5 cm, 0 cm and 5 cm.

material of the window needs to be selected with a high damage threshold, and KrF fused silica window can ensure a longer lifetime. Moreover, we found that the damage of the coating film on the window is on the vacuum side. We experimentally found that when the vacuum is on the order of 10^3 Pa, the window has a longer lifetime.

It can be seen in Fig. 5 that the spatial distribution of the laser pulse is not particularly uniform, which may be caused by dust on the surface of the window or different transmittance at different positions of the vacuum window.

To ensure that the position jitter of the laser is small, an optical image transport system is designed, which ensures that the free transport distance is very short. The test results of monitoring the position and energy of the laser for 1 h per day in different 10 days are shown in Fig. 6. It can be found that the RMS jitter of the laser position is less than 4 μm, and the RMS fluctuation of the laser energy is less than 0.5% (The pulse energy on the photocathode is set at around 50 μJ), which meets the requirements of the photocathode RF gun.

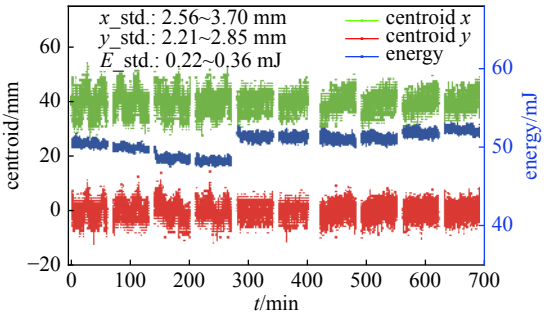

Fig. 6 Measurement results of laser pulse position and energy

3 Conclusion

The optical design and experimental studies on the spatiotemporal shaping of ps laser pulse are presented. 3 α-BBO crystals are used for temporal shaping and an aperture for spatial shaping. A quasi-uniform distribution in three-dimensional space of laser pulse is obtained. Using the image transport system, the final spatiotemporal shaped pulse can be transported to the photocathode at 6 m away from the aperture. In addition, the position and energy jitter of the drive laser at the virtual cathode are also measured. The experimental results show that the RMS jitter of the laser position is less than 4 μm, and the RMS jitter of the energy is less than 0.5%.

Reference:

[1] Akre R, Dowell D, Emma P, et al. Commissioning the linac coherent light source injector[J]. Physical Review Special Topics-Accelerators and Beams, 2008, 11: 030703.

[2] Zhu Pengfei, Zhu Y, Hidaka Y, et al. Femtosecond time-resolved MeV electron diffraction[J]. New Journal of Physics, 2015, 17: 063004.

[3] Xiang D, Fu F, Zhang J, et al. Accelerator-based single-shot ultrafast transmission electron microscope with picosecond temporal resolution and nanometer spatial resolution[J]. Nuclear Instruments and Methods in Physics Research Section A:Accelerators, Spectrometers, Detectors and Associated Equipment, 2014, 759: 74-82.

[4] Yang Jinfeng, Kondoh T, Kozawa T, et al. Pulse radiolysis based on a femtosecond electron beam and a femtosecond laser light with double-pulse injection technique[J]. Radiation Physics and Chemistry, 2006, 75(9): 1034-1040.

[5] Chen Han, Yan Lixin, Tian Qili, et al. Commissioning the photoinjector of a gamma-ray light source[J]. Physical Review Accelerators and Beams, 2019, 22: 053403.

[6] Kim K J. RF and space-charge effects in laser-driven RF electron guns[J]. Nuclear Instruments and Methods in Physics Research Section A:Accelerators, Spectrometers, Detectors and Associated Equipment, 1989, 275(2): 201-218.

[7] Serafini L, Rosenzweig J B. Envelope analysis of intense relativistic quasilaminar beams in rf photoinjectors: mA theory of emittance compensation[J]. Physical Review E, 1997, 55(6): 7565-7590.

[8] Schwarz J, Rambo P K, Smith I C, et al. Simple temporal pulse shaping using two Pockels cells[J]. Optical Engineering, 2005, 44: 094203.

[9] Sharma A K, Patidar R K, Raghuramaiah M, et al. Simple electro-optic technique to generate temporally flat-top laser pulses[J]. Optics Communications, 2011, 284(19): 4596-4600.

[10] Skeldon M D. Optical pulse-shaping system based on an electro-optic modulator driven by an aperture-coupled-stripline electrical-waveform generator[J]. Journal of the Optical Society of America B, 2002, 19(10): 2423-2426.

[11] Field J J, Durfee III C G, Squier J A, et al. Quartic-phase-limited grism-based ultrashort pulse shaper[J]. Optics Letters, 2007, 32(21): 3101-3103.

[12] Weiner A M. Femtosecond pulse shaping using spatial light modulators[J]. Review of Scientific Instruments, 2000, 71(5): 1929-1960.

[13] Weiner A M. Ultrafast optical pulse shaping: a tutorial review[J]. Optics Communications, 2011, 284(15): 3669-3692.

[14] Loos H, Dowell D, Gilevich S, et al. Temporal E-beam shaping in an S-band accelerator[C]//Proceedings of the 2005 Particle Accelerator Conference. 2005: 642-644.

[15] Vicario C, Ghigo A, Cialdi S, et al. Laser temporal pulse shaping experiment for SPARC photoinjector[R]. CARE-Conf-04-030-PHIN, 2004.

[16] Park Y, Asghari M H, Ahn T J, et al. Transform-limited picosecond pulse shaping based on temporal coherence synthesization[J]. Optics Express, 2007, 15(15): 9584-9599.

[17] Wang X T, Feng L, Lan T, et al. Drive laser temporal shaping techniques for Shanghai soft X-ray free electron laser[C]//39th International Free Electron Laser Conference. 2019: 466-468.

[18] Sharma A K, Tsang T, Rao T. Theoretical and experimental study of passive spatiotemporal shaping of picosecond laser pulses[J]. Physical Review Special Topics-Accelerators and Beams, 2009, 12: 033501.

[19] Wang Dong, Yan Lixin, Huang Wenhui. UV Pulse shaping with α-BBO crystals for the photocathode RF gun[C]//Proceedings of the 7th International Particle Accelerator Conference. 2016: 4079-4081.

[20] Laskin A, Laskin V. Imaging techniques with refractive beam shaping optics[C]//Proceedings of SPIE 8490, Laser Beam Shaping XIII. 2012: 84900J.

[21] Laskin A, Laskin V. Beam shaping in high-power laser systems with using refractive beam shapers[C]//Proceedings of SPIE 8433, Laser Sources and Applications. 2012: 84330N.

[22] Halavanau A, Ha G, Qiang G, et al. Microlens array laser transverse shaping technique for photoemission electron source[DB/OL]. arXiv preprint arXiv: 1609.01661, 2016.

[23] Jin Yuhua, Hassan A, Jiang Yijian. Freeform microlens array homogenizer for excimer laser beam shaping[J]. Optics Express, 2016, 24(22): 24846-24858.

[24] Tomizawa H, Dewa H, Taniuchi T, et al. Adaptive 3-D UV-laser pulse shaping system to minimize emittance for photocathode RF gun and new laser incidence system[C]//Proceedings of FEL. 2007: 298-305.

[25] Gross M, Qian H J, Boonpornprasert P, et al. Emittance reduction of RF photoinjector generated electron beams by transverse laser beam shaping[J]. Journal of Physics:Conference Series, 2019, 1350: 012046.

[26] Zhou Feng, Brachmann A, Emma P, et al. Impact of the spatial laser distribution on photocathode gun operation[J]. Physical Review Special Topics-Accelerators and Beams, 2012, 15: 090701.

光阴极微波电子枪驱动激光整形与传输系统

李 成， 汪文星， 李伟伟， 张浩然， 姜世民， 高攀云， 何志刚， 张善才

（中国科学技术大学 国家同步辐射实验室, 合肥 230029）

摘 要： 为满足合肥先进光源对高品质注入束流的要求，合肥先进光源预研项目研制了一套光阴极微波电子枪系统作为注入器电子源。为降低空间电荷效应引起的束流发射度增长，对驱动激光整形及传输系统进行了理论和实验研究。通过双折射晶体的脉冲时间整形以及采用光阑高斯截断的空间整形，得到了近似均匀分布的激光脉冲。像传递激光传输光路，实现了光阴极表面激光位置的高稳定性。实验结果显示，光阴极表面的激光位置抖动小于 4 μm，激光性能满足实验要求。

关 键 词： 光阴极微波电子枪；激光整形；双折射晶体；传输系统；发射度